Elsevier Editorial System(tm) for Continental Shelf Research
Manuscript Draft

Manuscript Number:

Title: Storm surges and atmospheric circulation: an analysis since 1950 for the Belgian coast and forecast for the 21th century

Article Type: Research Paper

Keywords: sea surges; sea-level pressure; climate change; North Sea; Belgian coast

Corresponding Author: M Albin Ullmann, PhD

Corresponding Author's Institution: KU Leuven

First Author: Albin Ullmann, Doctor

Order of Authors: Albin Ullmann, Doctor; Andreas Sterl, Doctor; Dries Van den Eynde, Doctor; Jaak Monbaliu, Doctor

Storm surges and atmospheric circulation: an analysis since 1950 for the Belgian coast and forecast for the 21th century

A. Ullmann[1] (*), A. Sterl (**), D. Van den Eynde (***), J. Monbaliu (*)

* Katholieke Universiteit Leuven, Hydraulics laboratory, Kasteelpark Arenberg 40, B-3001 Heverlee, Belgium

** Royal Netherlands Meteorological Institute, Global climate division, PO box 201 NL-3730 AE, De Bilt, the Netherlands

***Management Unit of the North Sea Mathematical Models (MUMM). Gulledelle 100, B-1200 Brussels

Submitted to Continental Shelf Research

[1] Corresponding author address: Albin Ullmann, Katholieke Universiteit Leuven, Hydraulics laboratory, Kasteelpark Arenberg 40, B-3001, Heverlee, Belgium (albin.ullmann@bwk.kuleuven.be).

Abstract

At daily time scale during the period 1950-2000, sea-surge heights at Oostende tide-gauge station are quasi-linearly correlated with the Sea-level pressure (SLP) over the Baltic Sea. High sea surges along the Belgian coast occur when a low pressure system remains stationary over Scandinavia and is associated with a reinforced Azores high. This SLP pattern favors strong onshore winds from Northwest sectors in the southern part of the North Sea, and the piling up of water along the Belgian coast. A statistical downscaling method is used to set-up a model to relate SLP to sea surge at Oostende. Linear regressions are designed to relate the daily surge height at Oostende with (i) the daily SLP over the Baltic Sea, (ii) the daily value of the pressure gradient between the Baltic Sea and the Azores and (iii) both of these atmospheric parameters. The multiple linear regression robustly reproduces the interannual to long-term variability of high surges at Oostende. This linear regression is then used with SLP time series simulated until 2100 under SRES scenario A1b, A2 and B2. High surges (at least up to the 99th percentile of the daily values) are expected to stay stationary during the 21st century, associated with no significant changes in SLP conditions over the Baltic Sea and over the Azores.

Key-words**:** sea surges, sea-level pressure, climate change, North Sea, Belgian coast

1. Introduction

Any rise in sea level will have adverse impacts (e.g. coastal erosion and flooding) that depend on the time scale and the magnitude of the rise, as well as the associated human response (Paskoff, 1993). In low coastal areas, vulnerability to short-term and long-term rise in sea level is particularly high (Nicholls *et al*., 1999). Recent climate models summarized by the Intergovernmental Panel on Climate Change (IPCC) have predicted a significant warming and global sea-level rise for the 21st century (IPCC, 2007), which is expected to increase the flooding risk along low lying coasts. Various factors may induce sea level variations at different time scales. On time scales longer than 1 year, regional and global scale sea level variations are related to volume change due to seawater density change, associated with temperature and salinity variations (Tsimplis and Rixen, 2002; Cazenaves and Nerem, 2004) and mass change between Ocean and continents, including ice melting (Lambeck, 1990; Cabanes *et al*., 2001). On time scales of less than 1 year, the predominant forcing of sea level variations is mostly related to atmospheric variability (Pirazzoli, 2000; Svensson and Jones, 2002; Wakelin *et al*, 2003; Ullmann et Moron, 2008). The atmospheric forcing leads to a sea surge defined as the difference between the observed sea level and the astronomical tide at the same moment. The mechanism leading to coastal floods is well known. Given the configuration of the coastline and the bathymetry, the severity of the sea surge depends mostly on wind speed and direction associated with moving mid-latitude low-pressure systems (Lamb, 1991; Pirazzoli, 2000, Woth *et al*., 2006).

The increase in storminess and surge height observed in the second half of the 20th century in the North Sea area has highlighted the current potential for high impact damage (WASA-group, 1998; Weisse *et al*., 2005). In recent years, many studies considered potential changes in sea surges in the North-Sea under climate change. Part of them, based on storm and wave models, show that an increase in extreme wind speed in the North Sea and the Norwegian Sea may take place under enhanced greenhouse gas conditions and could result in an increase in extreme surges (WASA-group, 1998; Woth *et al*., 2006; Debenard and Roed, 2008). However, other studies focusing on the Dutch coast foresee no significant changes in wind speed and sea-surge height until the end of the 21st century and for different climate change scenarios (Van den Hurk *et al*., 2007). Additionally, Debenard and Roed (2008) show that an increase in greenhouse gas concentration could lead to a significant increase in surge-height in the Skagerrak, but they do not predict significant changes in the southern part of the North Sea, especially along the Belgian and Dutch coast. In the same manner, Lowe *et al*. (2001) show a significant increase in extreme surges along a large proportion of the United Kingdom coastline in future climate. But they concluded that the pattern of change is spatially very inhomogeneous and increases do not occur in the southern North Sea region (Lowe *et al*., 2001). These discrepancies between different areas and between different studies lead to the conclusion that the resolution of regional climate models and of storm and wave models makes it difficult to interpret their results at small spatial scales like the Belgian coast, which extends only over 60 km only. Moreover, sea surges are regional-scale complex events depending on the coastal characteristics and especially on the link between the coastal orientation and the large-scale atmospheric pattern leading to onshore winds (Ullmann *et al*., 2008).

The purpose of our study is thus to develop a regional-scale strategy focused at the Belgian coast to (i) better understand the relationship between sea surges and the atmospheric circulation and (ii) to robustly predict the long-term variability of high surges in future climate. A downscaling approach is used to built a statistical model for a small-scale features (e.g. the surge) which are required by impact researchers but not adequately described in Global and Regional Circulation Models, with as input large-scale features, which are well resolved (von Storch, 1999). A downscaling approach is also used here to avoid the costly running of Regional Circulation and Hydrodynamic Models and to make the prediction of the impact of climate change on surge height for the Belgian coast easier, especially for impact researchers. After an overview of the data and methods used for this study (section **Error! Reference source not found.** and **Error! Reference source not found.**), the relationship between sea-level pressure (SLP) and sea surges along the Belgian coast is first analyzed at the daily time-scale during the 20th century (section **Error! Reference source not found.**). Following these relationship, linear statistical models are set-up to relate the interannual variability of surge height with SLP (section **Error! Reference source not found.**). The best statistical model is then used to forecast changes in surge height along the Belgian coast under A1b, A2 and B2 climate change scenario (section **Error! Reference source not found.**). Concluding remarks are provided in section **Error! Reference source not found.**.

2. Data

As the highest sea surges occur in winter, the October to March period ("winter" hereafter) is analyzed for each variable.

2.1. Sea level

This work analyses the daily maximum sea-level height time series at Oostende station ([02°55'E], [51°14'N]) along the Belgian coast from 1950 to 2000 (fig. 1). Sea level data are expressed in cm relatively to the same altimetric reference, the *Tweede Algemene Waterpassing*, indicated as TAW. For each daily maximum sea level (2 per day), the corresponding astronomical tide (in TAW) has been computed in a previous study by Technum-IMDC-Alkyon (2002). The daily surge height has been computed as the difference between the observed sea level and the astronomical tide at the same moment. As daily surges are derived from the daily maximum sea level, they always correspond to surges occurring during high tide which is particularly interesting from an impact perspective. For this study, we decided to use only the highest value of the two daily surges. Moreover, as the astronomical-tide height has been computed including the mean sea-level (MSL), interannual variability to long-term trend of surge are separated to the mean sea-level rise associated with the increase in ocean's volume. The different climatic aspects estimated this way are kept independent as much as possible and interannual variability to long-term trend of surge can be separated from ocean volume variations (Lowe *et al*., 2001; Pirazzoli *et al*., 2005).

2.2. Sea-level pressure

2.2.1. 20th century NCAR reanalysis

The mean sea level pressure (SLP) available from the National Center for Atmospheric Research (NCAR) at 12 UTC from October 1, 1950 to December 31, 2000 has been extracted from the NCAR web site (http://dss.ucar.edu/). No attempt has been made to fill the missing entries in the NCAR data or to remove the seasonal cycle.

2.2.2. GCM numerical simulation for the 20th and 21st century

- Two 6-hourly SLP time series simulated by ARPEGE-climat (coupled global circulation model) were provided by Meteo France (Royer *et al*., 2002). The first run simulates data from 1980 to 2100 and was driven by the scenario A2 of Greenhouse Gases (GHG) concentration from the IPCC Special Report on Emission Scenarios (SRES, Nakicenovic *et al*., 2000). This scenario assumes a rapid increase of the atmospheric

concentration of GHG until the end of the 21st century. The second run simulates data from 1950 to 2100 and was driven by the scenario B2 which is a more optimistic scenario than A2. In fact, this scenario predicts a rapid increase of the atmospheric concentration of GHG until 2050 but foresees then a small decline until the end of the 21st century, assuming a rapid development of sustainable and renewable energy. During the historical period, runs are forced by observed concentrations of GHG and anthropogenic aerosols. For the future, aerosols and solar irradiance are kept constant. Gridded-SLP data are extracted over [40°W-40°E]-[30°N-70°N] and interpolated on the same regular spatial resolution than the NCAR dataset.

- In the ESSENCE project (Sterl *et al*., 2008), the ECHAM/MPI-OM global climate model (Jungclaus et al., 2006) was used to create an ensemble of 17 runs over the period 1950-2100. For the 17-ensembles runs, the model has been driven by the same scenario but with 17 different initializations to make more robust estimates of the model's forced response compared to the natural chaotic climate variability. The model was forced by observed concentration of GHGs until 2000, while in the 21st century the forcing followed the SRES scenario A1b. Until 2050, the GHGs emissions in this scenario follows those in A2, but they stabilize after 2050. We here used the 6-hourly SLP fields for each of the 17 ESSENCE runs. Gridded SLP data are extracted over [40°W-40°E]-[30°N-70°N] and interpolated on the same regular spatial resolution as the NCAR dataset.

3. Sea surges and SLP for the 20th century: diagnostic analysis

Correlations between the daily surge height at Oostende station and the daily SLP (NCAR reanalysis) are first computed for each grid-point over [40°W-40°E]-[30°N-70°N] for the period 1950-2000. This method is used to analyze the relationship between the surge-height variability along the Belgian coast and the SLP variability over the Northern Atlantic and Europe at daily time scale. Figure 2 shows as quasi-linear relationship between the daily surge height at Oostende and the SLP over the Baltic Sea. Note that the correlation between the daily surge height at Oostende and the daily SLP over the Belgian coast is rather weak ($-0.3 < r < -0.2$; figure 2), meaning that surge height variability at Oostende is not directly linked with SLP variability over the Belgian coast. In other words, even if the inverted barometric effect (i.e. 1 cm surge-height variability for 1 hPa just-above SLP change) plays a role in the surge-height at daily time scale (Pirazzoli *et al*., 2005), it is not the main atmospheric forcing for surges at the Belgian coast.

Following Trigo and Davies (2002), a composite analysis is then performed to define the regional-scale atmospheric circulation associated with high surges. The composites of the mean SLP for each day, when the daily surges is above 35 cm (corresponding to the 90th percentile of daily surge height for the period 1950-2000), are computed for the following time lags: time 0 and time 0 minus 5, 4, 3, 2, 1 days (figures 3).When a surge event encompasses several days, the day with the highest surge is considered as day 0. Given that

definition, there are a total of 910 events, concentrated in the period between October and February. This composite analysis does not make any specific assumptions regarding the link between SLP and sea surges, but simply estimates the mean SLP pattern conditional on high surges.

For high surges and during the 6-days windows shown in figure 3, the main synoptic storm track in the North Atlantic–European sector follows a west to east axis, from the southern tip of Greenland (figure 3a) toward Scandinavia (figure 3f). During the same period, the low-pressure system intensifies, particularly from day(−2) to day(−1) (figure 3c-e), as it moves to the east. Associated with a reinforced Azores high, the Northeast-Southwest gradient across the North Sea is rather strong onward day(−1) (figure 3e). The low-pressure system typically reaches its minimum SLP over the northern tip of the Baltic Sea one day before the highest surge at Oostende. This SLP pattern favors strong onshore winds, from the Northwest sector in the southern North Sea, and the piling up of water along Belgian coast.

4. Sea surges and SLP: statistical downscaling for the 20th century

4.1. Methods and model set-up

There has been considerable interest and concern regarding the interannual and long-term variation of the amplitude of sea surges and their dependence on SLP variability. For example, studies focusing on the German Bight have demonstrated the strong link between the intramonthly percentiles of sea surges and the seasonal SLP over the eastern North Atlantic (e.g., Heyen *et al*., 1996; von Storch and Reichardt, 1997; Langenberg *et al*., 1999). Following results shown in section 3, a simple linear regression *(eq. 1)* is designed here for the period 1950-2000 to relate the daily surge height at Oostende to daily SLP averaged over the Baltic Sea ([15°E-20°E], [50°N-55°N]) which is the area where the SLP is the most strongly correlated with the surge height at Oostende at daily time scale (figure 2, section 3). A second simple linear regression *(eq. 2)* is then designed to relate the daily surge height at Oostende with the daily value of the pressure gradient between the SLP averaged over the Baltic Sea and the SLP averaged over the Azores ([30°W-0°W], [35°N-45°N]). In fact, this pressure gradient corresponds to the difference between the highest and the lowest SLP observed during high sea surges at Oostende and is clearly linked with the direction and strength of the strong surge-related atmospheric flow (figure 3f, section 3). Finally, a multiple linear regression *(eq. 3)* is finally tested in order to relate daily surge height at Oostende to both of these two atmospheric predictors:

$$DS_1 = (a_1 * BS) + cst_1 \qquad (1)$$

$$DS_2 = (b_1 * GRA\ ) + cst_2 \qquad (2)$$

$$DS_3 = (a_2 * BS) + (b_2 * GRA) + cst_3 \qquad (3)$$

Here the coefficients *a*, *b* and *cst* (i.e. constant value) are the regression coefficients, *DS* is the hindcast daily surge height (in cm), *BS* the daily sea-level pressure (in hPa) averaged over the Baltic Sea, and *GRA* the daily value of the pressure gradient (in hPa) between SLP averaged over the Baltic Sea and over the Azores for the period 1950-2000. In many applications, the predictor does not completely specify the predictand (von Storch, 1999). In a prediction perspective, hindcast time series need to have the same standard deviation as the observations. To meet this requirement, it has been proposed to inflate the hindcast by setting a coefficient of inflation (Karl *et al*., 1990). For each hindcast daily surge-height time series, a coefficient of inflation has been computed as the ratio between the standard deviation of observed and hindcast data. This technique has been used in the downscaling literature to some extent (e.g. Huth, 1999). After inflation, hindcast daily surge heights have the same standard deviation as *in situ* observations. All the coefficients are summarized in table 1.

For each hindcast daily surge-height time series, the monthly 90th (P90), 95th (P95) and 99th (P99) percentile of surge is computed and compared with *in situ* observation at Oostende. Percentile values are computed from a polynomial curve fit (6th order) to the empirical cumulative distribution function (cdf). We choose here the monthly 90th (95th and 99th) percentile of surge height, defined as the value for which 90 (95 and 99) percent of all daily surges are less than it, as an indicator of monthly high surges. We employ standard descriptive measures of goodness-of-fit, including the root-mean-square error (RMSE) to evaluate the accuracy of the simulated percentiles. RMSE represents overall error weighted by the square of deviations (von Storch and Zwiers, 1998). We also consider the linear correlation *r* between observed and simulated percentiles. The significance of the linear correlation is estimated with the random-phase test, first proposed by Janicot *et al*. (1996) and then elaborated by Ebisuzaki (1997). Mean and standard deviation (Std) of simulated and observed percentiles are also calculated. In a perfect simulation, in which simulations exactly match the observations, r=1 and RMSE=0. For inconsistent simulation, r ~ 0 and the RMSE can be up to twice the observed Std (von Storch and Zwiers, 1998). Linear trend of the monthly P90, P95 and 999 are also computed for the period 1950-2000 to test the performance of the three statistical models in long-term trends simulations.

4.2. Results

For the period 1950-2000, the mean of daily surges (including positive and negative surge values) is almost similar between hindcast and observations (table 2). At a daily time scale, the correlations between hindcast and observed daily surge height are almost similar. Nevertheless, regressions including the SLP averaged over the Baltic Sea (1 and 3) perform slightly better than the one employing only the pressure gradient (2) (figure 4; table 2). Moreover, it's interesting to note that the multiple linear regression doesn't perform better than the simple linear regression using SLP over the Baltic Sea (table 2). Daily surge-height

variability along the Belgian coast is thus mostly linked with the SLP variability over the Baltic Sea (table 2), consistent with results shown in section 3.

Monthly P90, P95 and P99 of surge are extracted for each daily surge-height time series computed with the three linear regressions and results are compared with observations at Oostende. The agreements between observed and hindcast monthly P90 is very strong for each linear regression (table 3). In fact, correlation coefficients are always > 0.73, which is significant at the 99% confidence level (table 3). Moreover, moderate RMSE indicates weak uncertainties about the individual hindcast (table 3). For high surges, the inverted barometric effect is not the main forcing of the surge amplitude but mostly the strength of the northeastward barometric gradient between low pressure over the Baltic Sea and high pressure over the Azores, which is directly linked with the direction and speed of northwesterly onshore winds over the Belgian coast (section 3). Nevertheless, statistical skills (correlation and RMSE) are always weakly lower when considering linear regression *(2)* using only the pressure gradient between the Baltic Sea and the Azores as the predictor. The statistical skills are almost similar for regressions *(1)* and *(3)* even if the coefficient of determination (r^2) of this last regression, which provides a measure of how well outcomes are likely to be predicted by the model, is 0.03 (3%) higher than the one for linear regression using only SLP over the Baltic Sea as the only predictor (table 3). Using both predictors (i.e. the SLP over the Baltic Sea and the pressure gradient between the Baltic Sea and the Azores) in the same linear regression doesn't significantly improve the simulation of the interannual variability of the monthly P90 for surges at Oostende compared to the simple linear regression using only SLP over the Baltic Sea as the predictor. The same results are valid when considering the monthly P95 and P99 (table 3). It means that from daily to interannual time-scale, the relationship between high surges and the pressure gradient is quasi exclusively linked with the SLP variability over the Baltic Sea and not with the SLP over the Azores. The agreements between observed and hindcast monthly P95 is still robust with significant correlation and moderate RMSE (table 3) but performances of each regression decrease for the simulation of monthly P99 (table 3). In fact, correlation between hindcast and observation significantly decrease, the RMSE reaches more than 20 cm and the standard deviation of hindcast values is underestimated (table 3). To summarize, a linear this statistical downscaling model performs well for the simulation of the interannual variability of high surges (e.g., surge occurring less than 2 days per month), which is particularly interesting for impact researchers such as coastal geomorphologist. Nevertheless, it usually underestimates the highest peaks. This is a recurring and normal property of linear statistical models. It could also mean that SLP over the Baltic Sea and the strength of the pressure gradient between the Baltic and the Azores can't completely explain the amplitude of highest surge peaks along the Belgian coast.

Linear trends are then computed from 1950 to 2000 with the monthly P90 simulated by the linear regressions *(1)* and *(3)*. Results are compared with the linear trend in P90 computed with in situ observation at Oostende station, equal to + 1.2 mm/year. When considering the linear regression *(1)* using only SLP averaged over the Baltic Sea as predictor, then the monthly P90 (P95 and P99) shows an insignificant increase of + 0.04 mm/year. The multiple linear regression *(3)*, using both SLP averaged over the Baltic Sea and the value of the

pressure gradient between the Baltic Sea and the Azores, shows a significant increase of the monthly P90 with a rate of + 1.1 mm/years, which is almost similar to the observed trend. The same results were found when considering P95 and P99 (not shown). Even if the SLP over the Azores doesn't play a role in the surge-height variability from daily to interannual time scale, it's seems to be a necessary predictor to simulate the long-term variability of surge height along the Belgian coast.

Climatically speaking, strong onshore winds leading to high surges along the Belgian coast are mainly generated by a strong Northeast-Southwest gradient between low pressure over the Baltic Sea and high pressure over the Azores. Daily to interannual variability of this pressure gradient is quasi exclusively associated with SLP variability over the Baltic Sea and not with SLP variability over the Azores. In fact, from daily to interannual time scales, SLP over the Azores is particularly stable associated with a large subtropical semi-permanent centre of high pressure, while SLP over the Baltic is strongly variable because it is under the main storm tracks (Rogers, 1997). Nevertheless, over the long-term, changes in the value of the pressure gradient between the Baltic Sea and the Azores could modify the frequency and strength of the surge-related atmospheric circulation over the North Sea. In fact, the increase of SLP over the Azores from 1960 to 1980, associated with positive deviation of the NOA (Lamb and Peppler, 1987), has increased the yearly frequency of strong northeast-southwest pressure gradient between the Baltic Sea and the Azores. Correspondingly, the amplitude of high surges at Oostende station has increased as well (Ullmann and Monbaliu, 2009). To summarize, high surges along the Belgian coast are mainly generated by stationary deep low pressure systems over the Baltic Sea and the associated northwesterly winds (i.e. winds turning anticlockwise around the low pressure system in the northern hemisphere). Over the long-term, SLP variability over the Azores also plays a role in the multi-decadal to secular surge-height variability. The multiple linear regression using both daily SLP over the Baltic Sea and the daily value of the pressure gradient between the Baltic Sea and the Azores as predictors of daily surge height at Oostende thus shows the best performance in simulating high surges variability, from daily time-scale to long-term trend.

4.3. Cross-validation

Following results shown in section 4.2., the multiple regression *(3)* can be easily used for hindcasting and predicting high surges along the Belgian coast. This regression is tested in cross-validation to avoid artificial skill due to 'overfitting' (Michaelsen, 1987; von Storch and Zwiers, 1998). Moreover, cross-validation is one approach to estimate how well the model we learned from training data is going to perform on future as-yet-unseen data. This is accomplished by dividing the SLP and the surge data into validation and learning subsets. The coefficient of the regression and the coefficient of inflation have been first learned for the period 1950-1974 and tested for the period 1975-2000. Learning and validation periods have then been reversed and all coefficients are summarized in table 4.

Figure 5 shows hindcast daily surge heights for the period 1975-2000 (1950-1974), based on regression coefficients derived from the learning period 1950-1974 (1975-2000). At the daily time scale, correlation between hindcast and *in situ* surge height at Oostende is significant (r = 0.61) at the 99% confidence level. Monthly P90 is then extracted from the inflated daily surge-height time series computed by the regression and compared with *in situ* observations at Oostende (figure 5 and table 5). The agreement between observed and hindcast monthly P90 is very strong. In fact, the intra-seasonal and intra-annual variability is correctly reproduced by our statistical model (figure 5). Moderate RMSE indicates weak uncertainties about the individual hindcasts (table 5). To conclude, the multiple linear regression can be used to predict future surge height with SLP simulated by climate models.

5. Statistical model: application to global climate models

5.1. Methods

In downscaling, small-scale phenomenon (i.e. weather variables or hydrodynamic phenomena) are related to large-scale quantities that are well resolved by GCMs like SLP. The multiple linear regression *(3)* is used with the daily SLP (12h UTC) from the GCM runs described in section 2.2.2. For each resulting daily surge-height time series, a coefficient of inflation is computed from the historical period with the same methodology shown before (section 4.1). Values are always between 1.59 and 1.6 which is almost similar to the coefficient of inflation computed for the period 1950-2000 from the observations (NCAR dataset). These results confirm that SLP variability is well simulated by the ECHAM/MPI-OM and ARPEGE climate models (Van Ulden and Van Oldenborgh, 2006). These coefficients of inflations are then used to inflate daily surge-height time series until 2100, assuming that future climate variability in A1b, A2 and B2 scenarios would not change the ratio between the standard of observations and simulations. Wintertime P90 of surge height are finally computed for each inflated daily surge-height time series and for the whole available period.

The Komolgorov-Smirnov test is one of the most useful and general methods for comparing two samples, as it is sensitive to differences in both location and shape of the empirical cumulative distribution functions of the two samples (Stephens, 1970). The null hypothesis of this test is that the two samples are drawn from the same distribution. In this case, the distributions considered under the null hypothesis are continuous distributions (Shorack and Wellner., 1986). The alternative hypothesis is that they have different continuous distributions. This test has the advantage of making no assumption about cumulative distribution function parameters and of giving a comparison between two samples based on the full distribution. First of all, the Komolgorov-Smirnov test is used on the historical period to compare the distribution of the observed and simulated wintertime P90 time series. The test is then used to compare the distribution of the wintertime P90 for the period 1950-2000 (1980-2000 for A2) and for the period 2050-2100 in order to analyze potential changes in

surge height along the Belgian coast. The advantage of this test is here to make a robust comparison between time series which don't have *a priori* the same chronology, i.e. observed and simulated wintertime P90 time series. In fact, all GCMs are chaotic (as well as the climate system) and cannot reproduce the real chronology of the climate variability except the chronology associated with external forcing as aerosol and Greenhouse gases.

5.2. Control experiment for the period 1950-2000

Simulated and observed wintertime P90 are compared during the period 1950-2000 (1980-2000 for A2) and show almost the same statistical skills (figure 6). The mean and the standard deviation are almost similar (table 6). Moreover, the Kolmogorov-Smirnov test doesn't show significant differences between hindcast and observed distributions of the wintertime P90. Results are similar when considering the P95 (not shown). It means that the multiple linear regression used with daily SLP simulated by ARPEGE and ECHAM/MPI-OM Global circulation models reproduces well the interannual variability of high surges at Oostende quite well.

5.3. Future surge height for the 21st century

For each runs, the wintertime P90 is averaged for three sub-periods: 1950-2000, 2001-2050 and 2051-2100 (table 7). Over the 21st century, the wintertime P90 of surges stay stationary along the Belgian coast for each climate change scenarios (figure 7 and 8). In fact, for each time series of wintertime P90, the Komolgorov-Smirnov test doesn't show significant changes in the distribution between the period 2051-2100 and 1950-2000. Moreover, linear trends of wintertime P90 computed for the period 2000-2100 never show significant rates neither within the 17-ensembles runs A1b nor in A2 and B2. For these last two scenarios, we keep in mind that only one single realization is used. Nevertheless, when using the ensemble members, results were almost similar for each of the 17 runs. Moreover, results are similar when considering the wintertime P95 and P99 (not shown). We conclude thus (i) that single runs give good estimates of the model's forced response and (ii) that future climate change, from optimistic to pessimistic scenario does not significantly modify sea-surge characteristics along the Belgian coast.

During the 21st century, wintertime mean SLP over the Baltic Sea (figure 9a) stays almost stationary in each of the 17-ensembles runs A1b (figure 9) as well as in A2 and B2 (not shown). Even if the daily to interannual variability of surge at Oostende is quasi exclusively associated with SLP variability over the Baltic Sea, the SLP variability over the Azores could play a role over the long-term by modifying the strength of the pressure gradient between the Baltic Sea and the Azores (Ullmann and Monbaliu, 2009). That's why it is important to have a large-scale view to analyze long-term changes in sea surges at local and regional scale (Ullmann and Moron, 2008). The SLP behavior near the Azores doesn't show significant

trends for the next century (figure 9b). Consequently, wintertime frequency of days associated with a strong pressure gradient between low pressure over the Baltic Sea and high pressure over the Azores stays stationary during the same period (figure 7c). Results are almost similar for A2 and B2 (not shown). To summarize, climate change in A1b, A2 and B2 SRES scenarios would not significantly modify the strength and the frequency of the surge-related North-Westerly atmospheric flow in the southern part of the North Sea over the 21st century.

6. Conclusion

At the daily time scale, sea-surge height at Oostende is quasi-linearly correlated with the SLP over the Baltic Sea. High surges along the Belgian coast are mainly associated with a low pressure system over Scandinavia and a reinforced Azores high. This atmospheric pattern leads to a strong Northeast-Southwest pressure gradient associated with onshore winds blowing from the Northwest sector in the southern part of the North Sea. Linear regressions are designed to relate the daily surge height at Oostende with *(1)* the daily SLP over the Baltic Sea, *(2)* the daily value of the pressure gradient between the Baltic Sea and the Azores and *(3)* both of these atmospheric parameters. Using both predictors (i.e. the SLP over the Baltic Sea and the pressure gradient between the Baltic Sea and the Azores) in a multiple linear regression reproduces well the variability of high surges from daily time-scale to long-term trend. This last regression, tested in cross validation, robustly reproduces the interannual variability of high surges at Oostende (P90 and P95). However, it usually underestimates the amplitude of highest surge peaks (e.g. the monthly P99). Therefore, studies needy of extreme values (e.g. return period calculation) require regional hydrodynamics models or more complex statistical methods for downscaling models.

The multiple linear regression is then used with a 17-runs ensemble A1b and with one A2 and one B2 SLP time series simulated until 2100. High surges (i.e. wintertime 90%, 95% and 99% percentile) stay stationary during the 21st century, associated with no significant changes in SLP conditions over the Baltic Sea and over the Azores. It means that climate change, from optimistic to pessimistic SRES scenarios, would obviously not significantly modify the strength and frequency of north westerly winds in the southern part of the North Sea. This result is based on a linear statistical downscaling between SLP and surge height designed in the 20th century, assuming that future climate variability won't change the relationship between the predictors (i.e. SLP) and the predictands (i.e. the surge height at Oostende). This is an imponderable assumption in all climate forecasting using a downscaling approach. The stationary amplitude of high surges for the 21st century presented in this paper is consistent with results found by Lowe *et al*. (2001) and Van den Hurk *et al*. (2006) showing no significant changes in wind speed and sea surge along the Dutch coast and in a large portion of the United Kingdom coastline in a future climate. Moreover, these results confirm that climate change would not significantly modify high surges and winds in the southern part of the North Sea region (Debenard *et al*., 2002). The main advantage of using the linear statistical downscaling model designed here, is that it can be easily used with other Global Circulation Models and with other climate change scenarios and as such can help in the

estimation of high surges which is required for impact calculation especially for coastal erosion and sedimentary transport.

Acknowledgements

This study is partly funded by the European Commission 2005-2009 under SEAMOCS (Applied stochastic models for ocean engineering, climate and safe transportation) Research Training Network. This study is also part of the QUEST4D project (Quantification of erosion and sedimentation patterns to trace the natural versus anthropogenic sediment dynamics) funded by the Belgian Science Policy. The ESSENCE project, lead by Wilco Hazeleger (KNMI) and Henk Dijkstra (UU/IMAU), was carried out with support of DEISA, HLRS, SARA and NCF (through NCF projects NRG-2006.06, CAVE-06-023 and SG-06-267). We thank the DEISA Consortium (co-funded by the EU, FP6 projects 508830 / 031513) for support within the DEISA Extreme Computing Initiative (www.deisa.org). The authors thank Camiel Severijns (KNMI) and HLRS and SARA staff for technical support.

Reference

Butterworth S., 1930. On the theory of filter amplifiers. *Wireless Engineer*, 7, 536-541.

Cabanes C., Cazenave A., Le Provost C., 2001. Sea level rise during past 40 years determined from satellite and in situ observations. *Science*, 294, 840-842.

Cazenave A., Nerem R.S., 2004. Present-day sea level change: observations and causes. *Reviews of Geophysics*, 42, RG3001, doi: 10.1029/2003RG00139.

Debernard J., Roed L.P., 2008. Future wind, wave and storm surge climate in the Northern Seas: a revisit. *Tellus*, 60, 427-438.

Debenard J., Saetra O., Roed L.P., 2002. Future wind, wave and storm surge climate in the northern North Atlantic. *Climate Research*, 23, 39-49.

Ebisuzaki W., 1997. A method to estimate the statistical significance of a correlation when the data are serially correlated. *Journal of Climate*, 10, 2147-2153.

Heyen H., Zorita E., von Storch H., 1996. Statistical downscaling of monthly mean North-Atlantic air pressure to sea level anomalies in the Baltic Sea. *Tellus*, 48A, 312-323.

Huth R., 1999. Statistical downscaling in central Europe: evaluation of methods and potential predictors. *Climate Research*, 13, 91-101.

IPCC, 2007. Climate Change 2007. The Physical Science Basis. *Cambridge University Press*, Cambridge, 940 p.

Janicot S., Moron V., Fontaine B., 1996. Sahel droughts and ENSO dynamics. *Geophysical Research Letter*, 23, 515-518.

Jungclaus J.H., Botzet M., Haak H., Keenlyside N., Luo J.J., Latif M., Marotzke J., Mikolajewicz U., Roeckner E., 2006. Ocean circulation and tropical variability in the coupled model ECHAM5/MPI-OM. *Journal of Climate*, 19, 3952-3972.

Karl T.R., Wang W.C., Schlesinger M.E., Knight R.W. Portman D., 1990. A method of relating general circulation model simulated climate to observed local climate. Part I: Seasonal statistics. *Journal of Climate*, 3, 1053-1079.

Lamb P.J., Peppler R.A., 1987. North Atlantic Oscillation: concept and application. Bulletin of the American Meteorological Society, 68, 1218-1225.

Lambeck C., 1990: Late Pleistocene, Holocene and present sea-levels: constraints on future change. *Global and Planetary Change*, 3, 205-217.

Langenberg H., Pfizenmayer A., Von Storch H., Sundermann J., 1999. Storm-related sea level variations along rthe North Sea coast: natural variability and anthropogenic change. *Continental Shelf Research.* 19, 821-842.

Lamb H., 1991. Historic Storms of the North Sea, British Isles and Northwest Europe. *Cambridge University Press*, Cambridge, 204 pp.

Lowe J.A., Gregory J.M, Flather R.A., 2001. Changes in the occurrence of storm surge in the United Kingdom under a future climate scenario using a dynamic storm surge model driven by the Hadley Center climate models. *Climate Dynamics*, 18, 197-188.

Michaelsen J.M., 1987. Cross-validation in statistical climate forecast models. *Journal Of applied Meteorology*, 26, 1589-1600.

Nakicenovic N., et al., 2000. Special Report on Emissions Scenarios: A Special Report of Working Group III of the Intergovernmental Panel on Climate Change. Cambridge University Press, Cambridge, U.K. 599pp. Avalable online at: www.grida.no/climate/ipcc/emission/index.htm.

Nicholls R.J., Hoozemans F.M.J., Marchand M., 1999. Increasing flood risk and wetland losses due to global sea-level rise: regional and global analyses. *Global Environnmental Change*, 9, 69-87.

Paskoff R., 1993. Côtes en danger. Pratiques de la Géographie. Masson Eds. 247 p.

Pirazzoli P.A., Costa S., Dornbusch U., Tomasin A., 2005. Recent evolution of surge-related events and assessment of coastal flooding risk on the eastern coasts of the English Channel. *Ocean Dynamics*, Special Issue, mars 2006, 56, 498-512.

Pirazzoli P.A., 2000. Surges, atmospheric pressure and wind change and flooding probability on the Atlantic coast of France. *Oceanologica Acta,* 23, 643-661.

Rogers J.C., 1997. North Atlantic storm track variability and its association to both North Atlantic Oscillation and climate variability of Northern Europe. Journal of Climate, 10, 1635-1647.

Royer J.F., Cariolle D., Chauvin F., Déqué M., Douville H., Hu R.M, Planton S., Rascol A., Ricard J.L., Melia D.S.Y., Sevault F., Simon P., Somot S., Tyteca S., Terray L., Valcke S., 2002. Simulation des changements climatiques au cours du XXI^{ème} siècle incluant l'ozone stratosphérique. *Compte Rendus Geoscience*, 334: 147-154.

Shorack G.R, Wellner J.A., 1986. Empirical Processes With Applications to Statistics, John Wiley & Sons Inc, 976 p. (ISBN 047186725X).

Stephens M. A., 1970. Use of the Kolmogorov-Smirnov, Cramer-Von Mises and Related Statistics Without Extensive Tables. *Journal of the Royal Statistical Society*. Series B, Vol. 32, No. 1, pp. 115–122.

Sterl A., Severijns C., van Oldenborgh G.J., Dijkstra H., Hazeleger W., van den Broeke M., Burgers G., van den Hurk B., van Leeuwen P.J., van Velthoven P., 2008. When can we expect extremely high surface temperatures? *Geophys. Res. Lett.*, 35, L14703 doi: 10.1029/2008GL034071

Svensson C., Jones D.A., 2002. Dependence between extreme sea surge, river flow and precipitation in eastern Britain. *International Journal of Climatology,* 22, 1149-1168.

Technum-IMDC-Alkyon, 2002. Hydrodynamic boundary conditions for the water levels and storm surge conditions to support the redesign of the coastal protection and to increase the harbor access at Ostend (in Dutch). *Study report for the Flemish Government of Belgium*, Administration AWZ Afdeling Waterwegen Kust.

Trigo I.F., Davies T.D., 2002. Meteorological conditions associated with sea surges in Venice: A 40 year climatology. *International Journal of Climatology,* 22, 787-803.

Tsimplis M.N., Rixen M., 2002. Sea level in the Mediterranean Sea: the contribution of temperature and salinity changes. *Geophysical Research Letters*, 29, 1-4, doi: 10.1029 / 2002GL015870.

Ullmann A., Monbaliu J., 2009. Changes in atmospheric circulation over the North Atlantic and sea surge variations along the Belgian coast during the 20th century. *International Journal of Climatology*. Doi: 10.1002/joc.1904

Ullmann A. Moron V., 2008. Weather regimes and sea surge variations over the Gulf of Lions during the 20th century. *International Journal of Climatology*, 28, 159-171.

Ullmann A., Pirazzoli P.A, Moron V., 2008**.** Sea surges around the Gulf of Lions and atmospheric conditions. *Global and Planetary Change*, 63: 203-214.

Van den Hurk B., Klein Tank A., Lenderink G., van Ulden A., van Oldenborg G.J., Katsman C., van den Brink H., Keller F., Bessembinder J., Burgers G., Komen G., Hazelegers W., Drifhout S., 2007. KMNI New climate Change scenarios for the Netherlands. *Water Science and Technology*, 56, 27-33, doi: 10.2166/wst.2007.533.

Van Ulden A., Van Oldenborgh G.J., 2006. Large-scale atmospheric circulation biases and changes in global climate model simulations and their importance for regional climate scenarios: a case of study for West-Central Europe. Atmospheric Chemistry and Physics, 6, 863-881.

Von Storch H., 1999. On the use of "inflation" in statistical downscaling. *Journal of Climate*, 12, 3505-3506.

Von Storch H., Zwiers F.W., 1998. Statistical analysis in climate research. *Cambridge Univ. Press*. 494 p.

Von Storch H., Reichardt H., 1997. A scenario of storm surge statistics for the German bight at the expected time of doubled atmospheric Carbon Dioxide concentration. *Journal of Climate*, 10, 2653-2662.

Wakelin S.L., Woodworth P.L., Flather R.A., Williams J.A., 2003. Sea-level dependence on the NAO over the NW European continental shelf, *Geophysical Research Letters*, 30, doi:10.1029/2003GLO17041.

WASA group, 1998. Changing waves and storms in the Northeast Atlantic ? *Bulletin of American Meteorological Society*, 79, 741-760.

Weisse R., Von Storch H., Feser F., 2005. Northeast Atlantic and North Sea storminess as simulated by regional climate model 1958-2001 and comparison with observations. *Journal of Climate*, 18, 465-479.

Woth K., Weisse R., Von Storch H., 2006. Climate change and North Sea storm surge extremes: an ensemble study of storm surge extremes expected in a changed climate projected by four different regional climate models. *Ocean Dynamics*, 56, 3-15.

Figures and table captions

Figure 1. Location of Oostende tide-gauge station

Figure 2. Correlation between daily surge height at Oostende and the daily SLP for the period 1950-2000 (October to March). Positive (negative) correlations are drawn in full (dashed) line.

Figure 3. Composite of SLP calculated at time lag of (a) 5 days, (b) 4 days, (c) 3 days, (d) 2 days, (e) 1 days and (f) no lag for surges > 35 cm at Oostende on October-March period from 1950 to 2000.

Figure 4. Scatter plot between daily surge height observed at Oostende and daily surge height simulated with the linear regression using (a) the daily SLP averaged over the Baltic Sea, (b) the daily value of the pressure gradient between the SLP averaged over the Baltic Sea and over the Azores and (c) both of these two atmospheric index as the predictor and after inflation.

Figure 5. Time series of the monthly 90^{th} percentile of surge at Oostende station as derived from *in situ* observation (full line) and estimated (dashed line) with the linear regression using daily SLP averaged over the Baltic Sea and the daily value of the pressure gradient between the Baltic Sea and the Azores as predictors of daily surge height and after inflation (a) When the regression is learned for the period 1950-1974 and tested for the period 1975-2000. (b) When the regression is learned for the period 1975-2000 and tested for the period 1950-1974.

Figure 6. Box plot of the wintertime 90% percentile of surges observed at Oostende (Obs.) and for the 17- ensembles runs A1b and for B2 and A2 for the period 1950-2000 (1980-2000 for A2). With the five-number summaries: the smallest observation, lower quartile, median, upper quartile and the largest observation.

Figure 7. Thin line: mean of the 17-ensembles time series (A1b) of wintertime 90^{th} percentile of sea surges for the period 2000-2100. Bold line: 30 year low-pass variations using a recursive low-pass Butterworth filter (Butterworth, 1930). The gray shading represents the variability within the 17-ensembles time series in each winter (i.e. the yearly mean +/- σ).

Figure 8. Thin line: time series of wintertime 90^{th} percentile of surge for the period 2000-2100. Continuous line for A2 and dashed line for B2 climate change scenarios with 30 year low-pass variations using a recursive low-pass Butterworth filter (Butterworth, 1930) as superimposed bold lines.

Figure 9. Thin line: average of the 17-ensembles time series of wintertime mean SLP (a) over the Baltic Sea ([15°E-20°E], [50°N-55°N]), (b) over the Azores ([30°W-0°W], [35°N-45°N]) and (c) of the frequency of daily SLP over the Baltic Sea < 990 associated with SLP > 1020 over the Azores (2000-2100). Bold line: 30 year low-pass variations using a recursive low-pass Butterworth filter

(Butterworth, 1930). The gray shading represents the variability within the 17-ensembles time series in each year (i.e. the yearly mean +/- σ).

Table 1. Coefficients of the regressions (*a*, *b* and *cst*) and coefficient of inflation (*IF*). Regression *(1)*: for the linear regression using daily SLP averaged over the Baltic Sea as the predictor of daily surge height during the period 1950-2000. Regression *(2)*: for the linear regression using daily value of the pressure gradient between the Baltic Sea and the Azores as the predictor of daily surge height during the period 1950-2000. Regression *(3)*: for the multiple linear regression using both predictor *(1)* and *(2)* during the period 1950-2000.

Table 2. First line: the mean daily surge height at Oostende (including positive and negative surges) computed for the period 1950-2000 with *in situ* observation and with the daily surge height simulated with the regression *(1)* using the daily SLP averaged over the Baltic Sea, *(2)* the daily value of the pressure gradient between the SLP averaged over the Baltic Sea and over the Azores and *(3)* both of these two atmospheric indexes as predictors and after inflation. Second line: correlation between daily observed surge height at Oostende and daily surge height computed with linear regression with *(1)*, *(2)* and *(3)* and after inflation during the period 1950-2000.

Table 3. Goodness-of-fit statistics of the monthly 90th (P90), 95th (P95), and 99th (P99) percentile estimated with linear regressions and after inflation for the period 1950-2000. Regression *(1)*: with daily SLP averaged over the Baltic Sea as predictors of daily surge heights. Regression *(2)*: with daily value of the pressure gradient between the SLP averaged over the Baltic Sea and the Azores as predictors of daily surge height. Regression *(3)*: with both of these two atmospheric indexes as the predictors. Two (three) stars indicate that the correlation is significant at the 95% (99%) confidence level.

Table 4. Coefficients of the regressions (*a*, *b* and *cst*) and coefficient of inflation (*IF*) for the regression (3). Second line: when the coefficient of the regression are learned for the period 1950-1974.Third line: when the coefficient of the regression are learned for the period 1975-2000.

Table 5. Goodness-of-fit statistics of the monthly 90th percentile of surge estimated with the linear regression using daily SLP averaged over the Baltic Sea and daily value of the pressure gradient between the Baltic Sea and Azores as predictors of daily surge height and after inflation. In second line (third line), when the regression is learned for the period 1950-1974 (1975-2000) and tested for the period 1975-2000 (1950-1974). With the linear correlation (r), the roots mean square error (RMSE) and the standard deviation (Std). Three stars indicate the two-sided 99% level of significance according to a random-phase test.

Table 6. Mean, standard deviation (Std.), maximum (Max.) and Minimum (Min.) wintertime 90th percentile of sea surges observed at Oostende and for the 17-ensembles runs A1b and for B2 and A2 for the period 1950-2000 (1980-2000 only for A2).

Table 7. Wintertime 90th percentile of surge observed at Oostende station and for the 17-ensembles runs A1b and the two single B2 and A2 daily sea surge time series. Wintertime 90th percentile are averaged for three sub-periods: 1950-2000 (1980-2000 only for A2), 2001-2050 and 2051-2100.

Albin Ullmann
Katholieke Universiteit te Leuven,
Katseelpark Arenberg
3001 Leuven Belgium.

Leuven, May 13 2009

To editor of Continental Shelf Research

Dear Editor,

Please find attached the manuscript we would like to submit to your journal. The title is "Storm surges and atmospheric circulation: an analysis since 1950 for the Belgian coast and forecast for the 21th century". This paper focuses on the understanding and the prediction of the long-term variability of storm-surges along the Belgian coast under A1b, A2 and B2 climate change scenario.

We are looking forward to any comment about our paper.

Best Regards,

Albin Ullmann

Jaak Monbaliu

Figure 1

Click here to download high resolution image

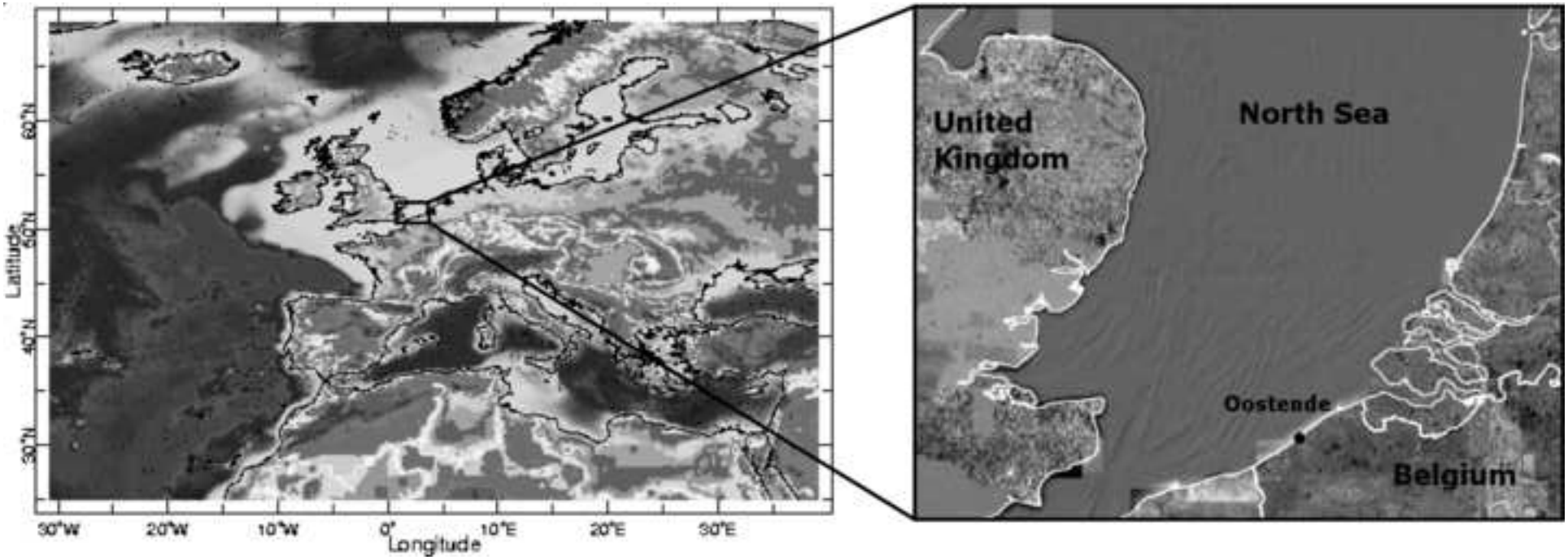

Figure 2

Click here to download high resolution image

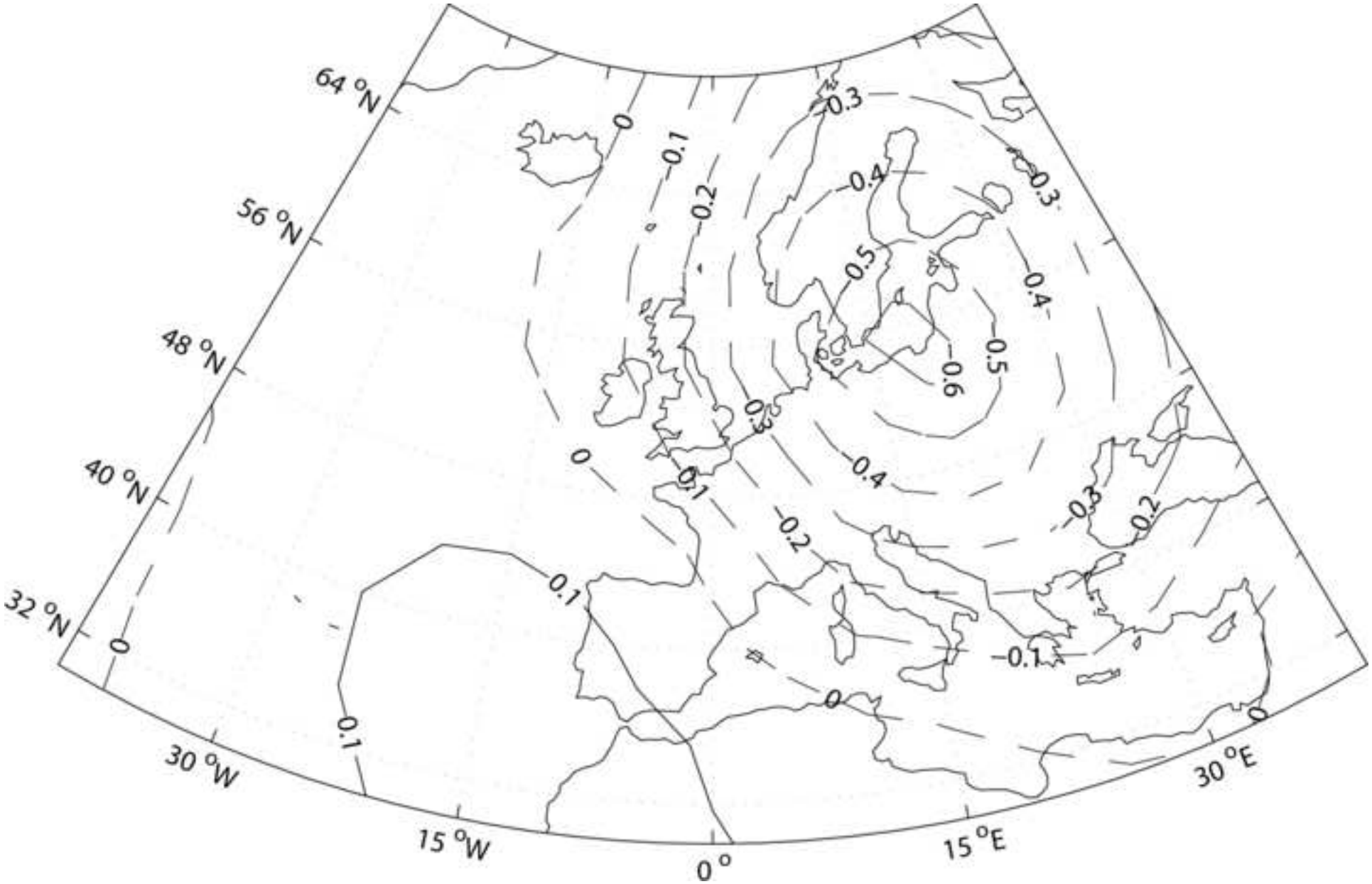

Figure 3

Click here to download high resolution image

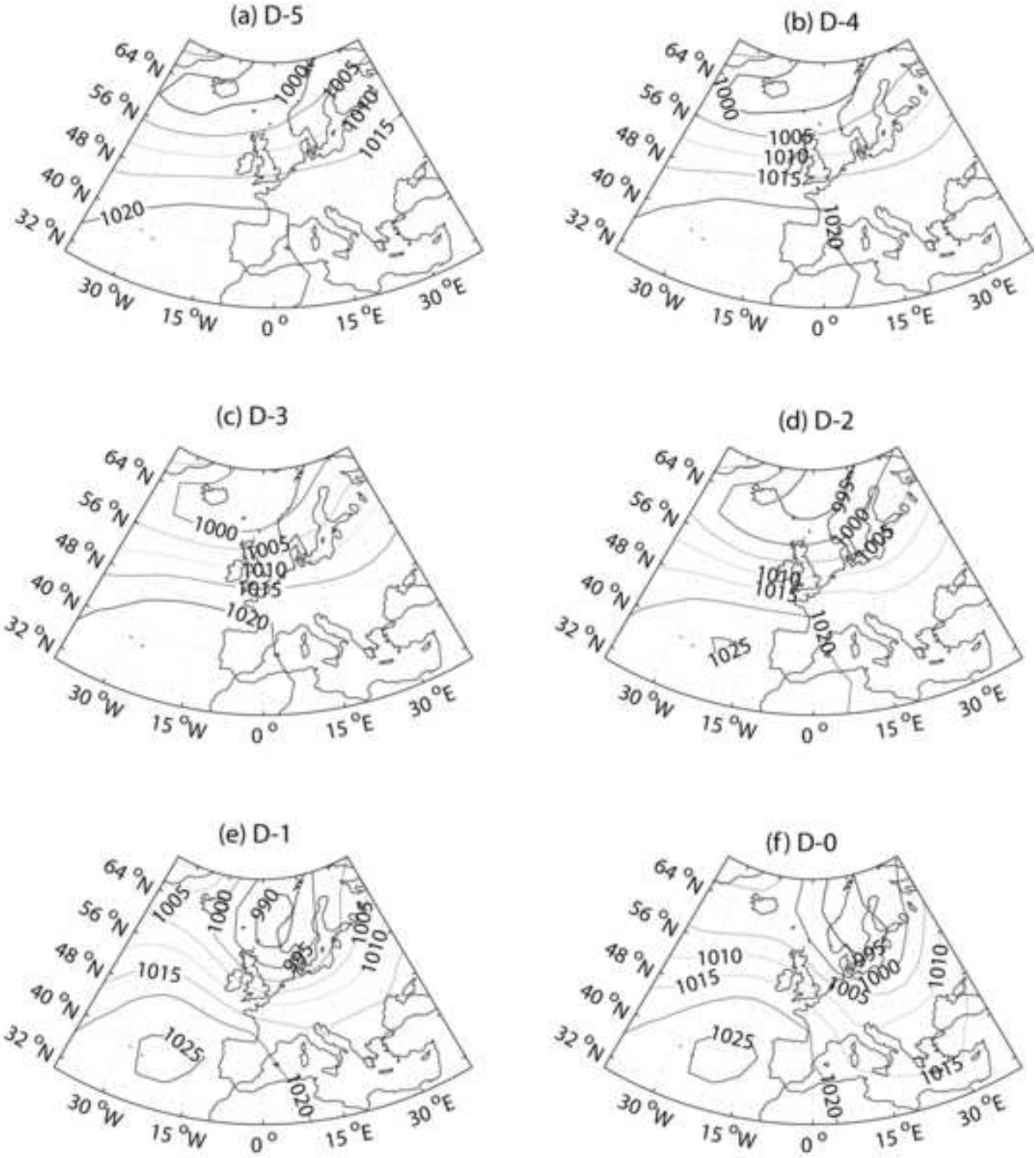

Figure 4

Click here to download high resolution image

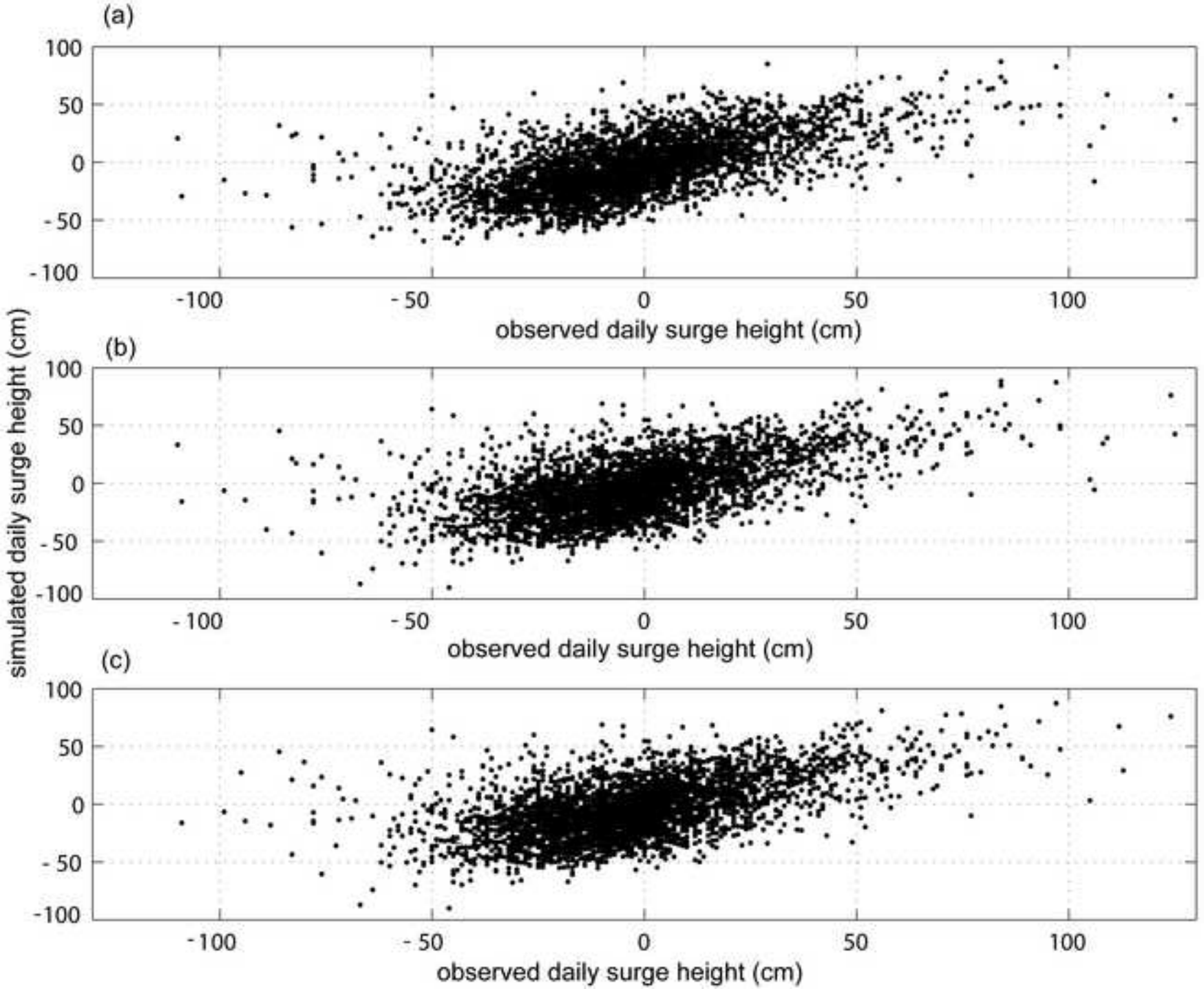

Figure 5

Click here to download high resolution image

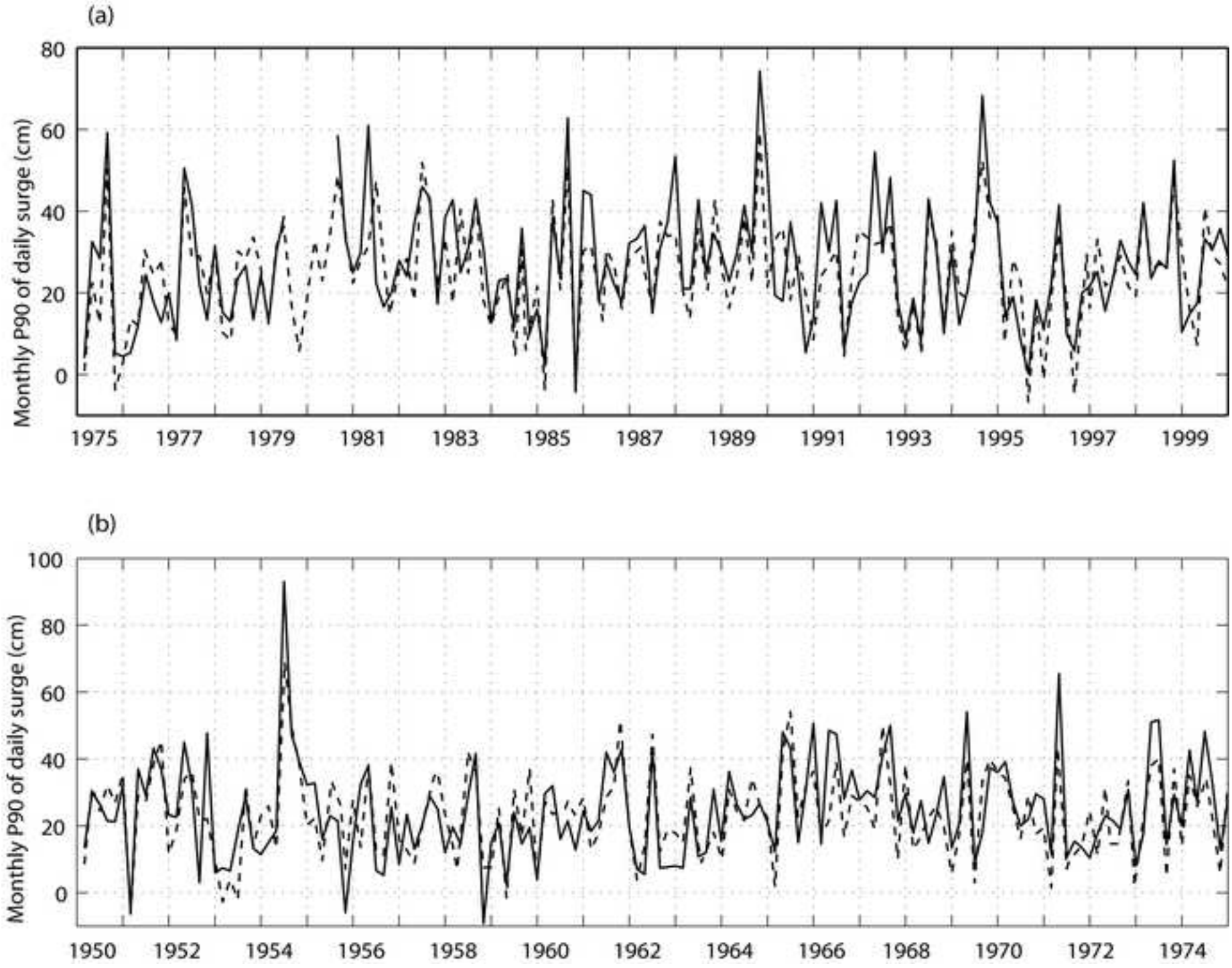

Figure 6

Click here to download high resolution image

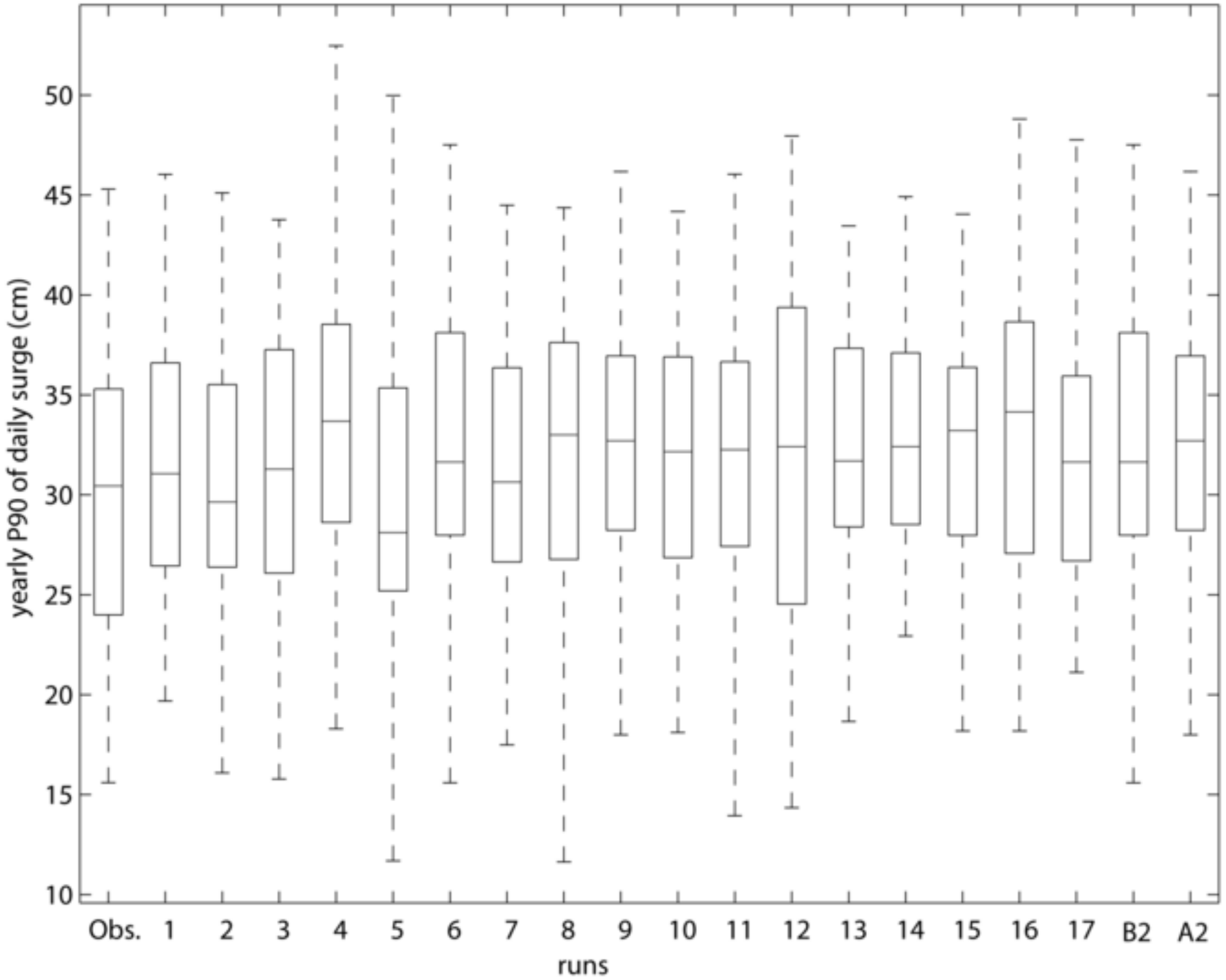

Figure 7

Click here to download high resolution image

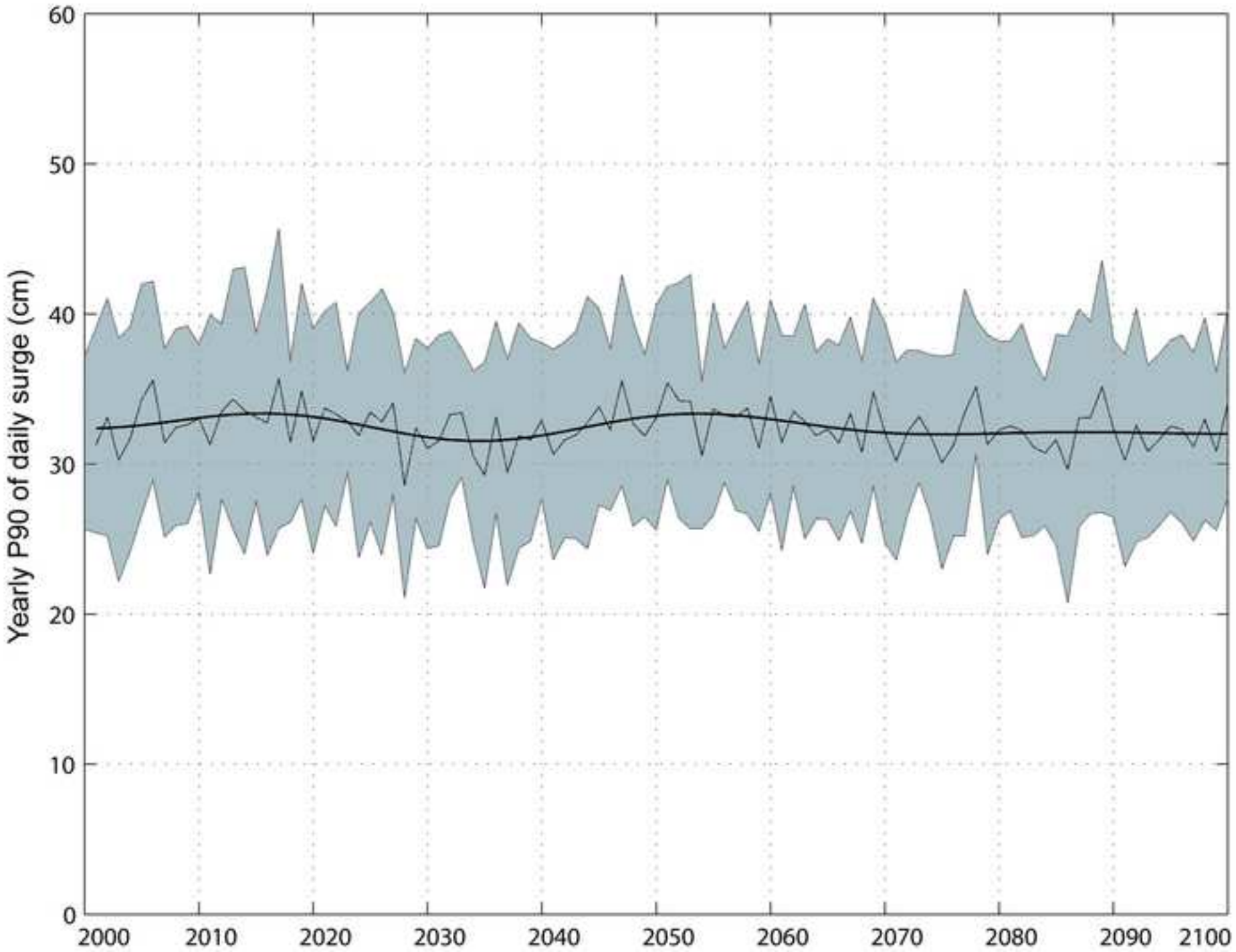

Figure 8

Click here to download high resolution image

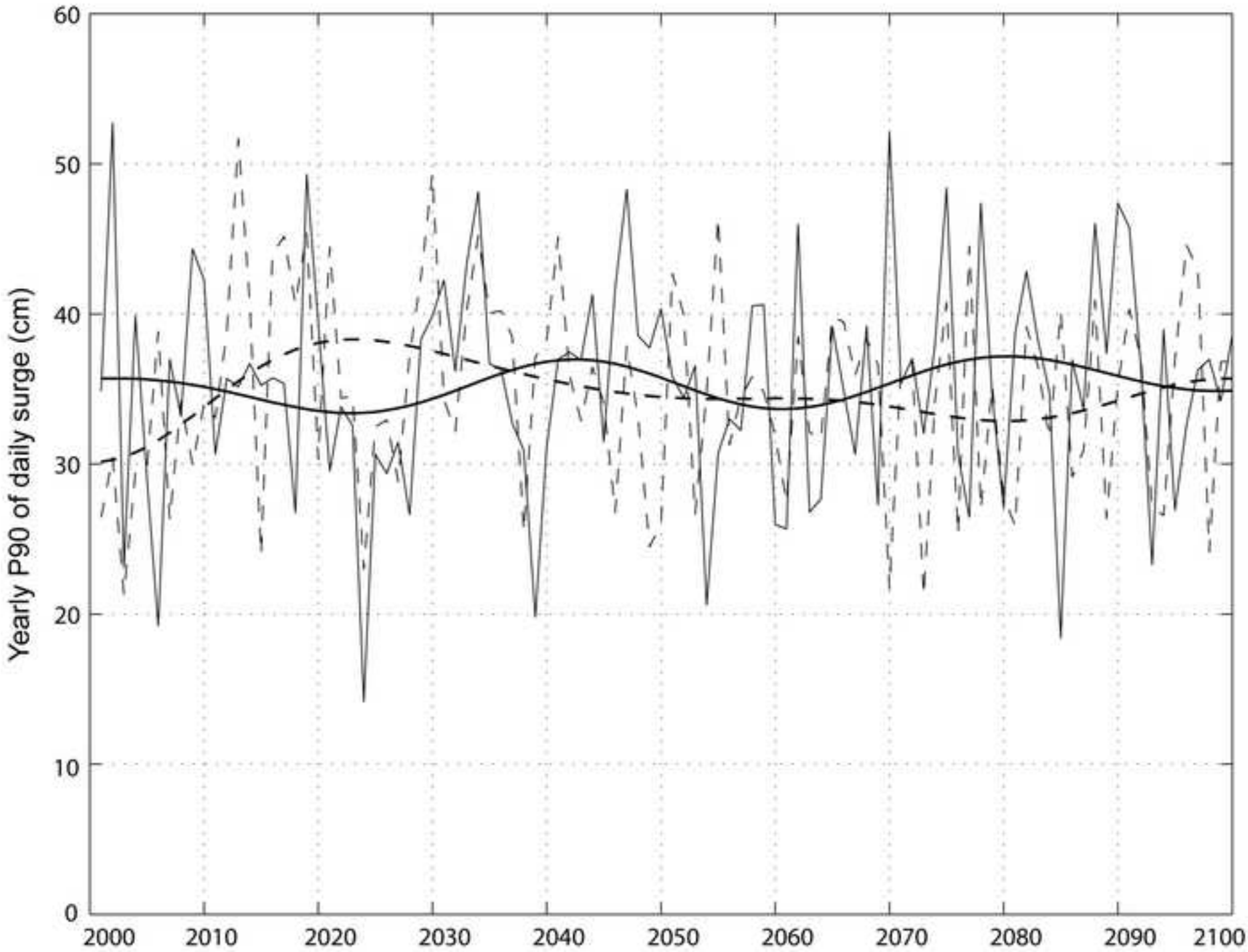

Figure 9

Click here to download high resolution image

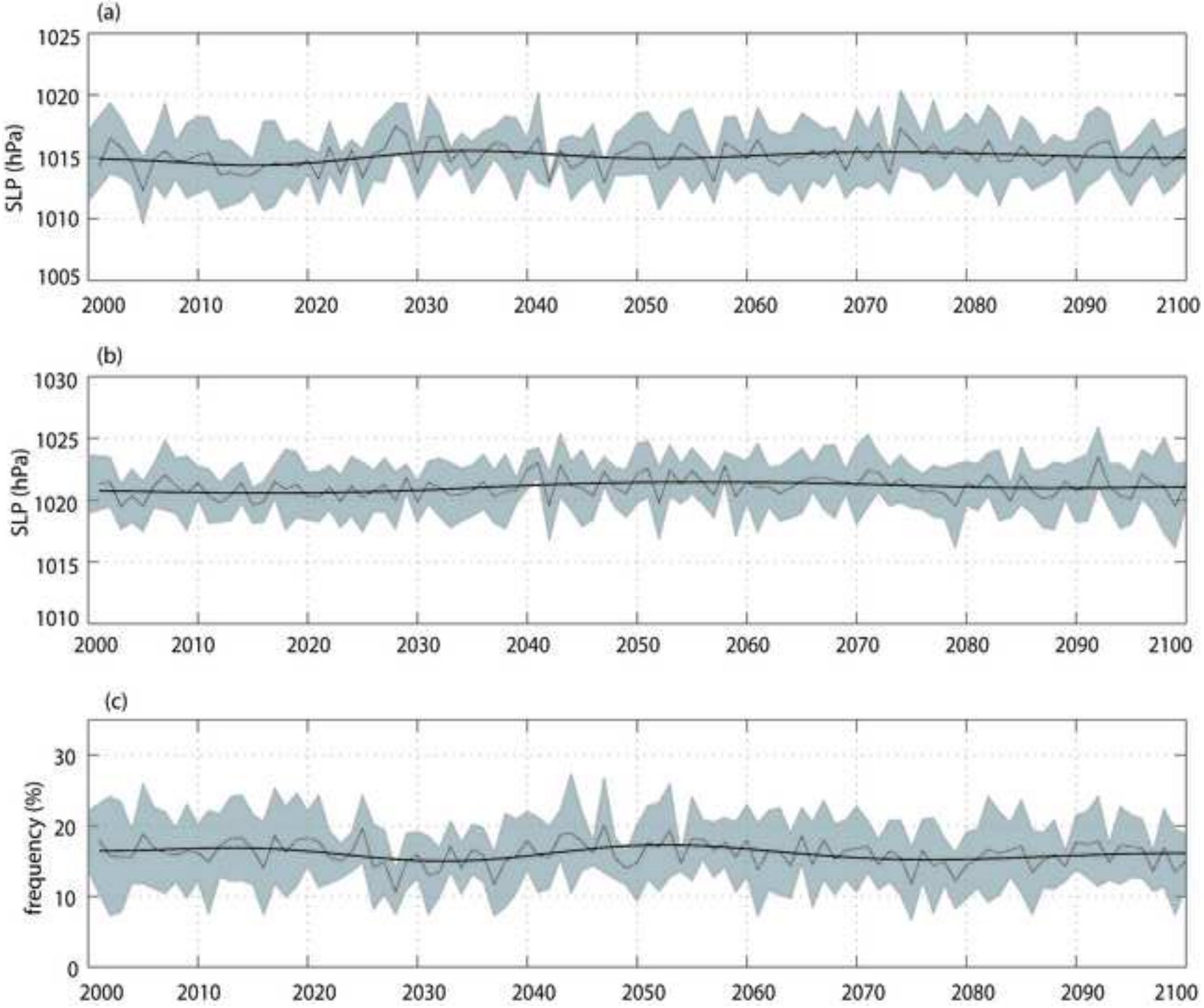

Table 1

Click here to download high resolution image

Regression *(1)*			
a_1	cst_1	IF_1	
-1.2	1182.2	1.66	
Regression *(2)*			
b_1	cst_2	IF_2	
-0.92	-7.47	1.76	
Regression *(3)*			
a_2	b_2	cst_3	IF_3
-0.89	-0.26	899.4	1.65

Table 2

Click here to download high resolution image

	Oostende obs.	Regression *(1)*	Regression *(2)*	Regression *(3)*
Mean of daily surge	-2.8 cm	-3.4 cm	-3.1 cm	-3.4 cm
r obs. vs hindcast		0.61***	0.56***	0.61***

Table 3

Click here to download high resolution image

	r (observation vs simulation)	RMSE (cm)	Mean (cm)		Std. (cm)	
			Obs	Sim	Obs	Sim
Monthly P90						
regression (1)	0.75***	9.1	23.19	23.6	13	13.1
regression (2)	0.73***	11	23.19	21.3	13	16.1
regression (3)	0.77***	9.1	23.19	23.4	13	14.5
Monthly P95						
regression (1)	0.65***	14.1	34.5	30.4	17.3	15.1
regression (2)	0.63***	14.3	34.5	28.3	17.3	16.7
regression (3)	0.68***	13.7	34.5	30.6	17.3	15.5
Monthly P99						
regression (1)	0.49**	22.6	51.5	39.2	25.5	17.3
regression (2)	0.51**	22.7	51.5	38.3	25.5	18.8
regression (3)	0.57**	20.1	51.5	42.1	25.5	18.7

Table 4

Click here to download high resolution image

	a	*b*	*cst*	*IF*
1950-1974	-0.96	-0.22	968.3	1.65
1975-2000	-0.83	-0.31	842.5	1.66

Table 5

Click here to download high resolution image

	r (observation vs simulation)	RMSE (cm)	Mean (cm)		Std. (cm)	
			Obs	Sim.	Obs .	Sim.
P90 (1975-2000)	0.76***	7.9	32.1	30.2	14.2	14.8
P90 (1950-1974)	0.72***	7.6	28.2	26.8	13.5	13.9

Table 6

Click here to download high resolution image

	Mean (cm)	Std. (cm)	Max. (cm)	Min. (cm)
Oostende	30.1	7.1	45.2	15.3
A1b 17 runs	32.3	7.8	57.3	12.2
A2	32.2	7.2	46	17.1
B2	31	7.4	47.3	16.2

Table 7

Click here to download high resolution image

	1950-2000	2001-2050	2051-2100
Oostende Obs.	30.2		
Run 1	31.5	31.3	31.2
Run 2	30.6	32.1	31.8
Run 3	31.7	31.9	31.2
Run 4	33.8	35.0	31.0
Run 5	28.7	34.8	31.8
Run 6	32.4	29.4	32.0
Run 7	31.3	31.8	32.5
Run 8	32.1	33.4	31.2
Run 9	31.9	31.3	32.1
Run 10	31.7	33.4	30.5
Run 11	31.4	32.5	32.3
Run 12	32.0	32.6	31.6
Run 13	32.3	31.8	31.4
Run 14	32.8	33.0	32.1
Run 15	32.3	30.8	31.4
Run 16	33.5	32.3	32.3
Run 17	31.6	32.8	32.6
A2	31.2	35.2	31.8
B2	32.1	34.1	33.3